

PIECEWISE POLYNOMIAL REGRESSION OF TAME FUNCTIONS VIA INTEGER PROGRAMMING

GILLES BAREILLES[†], JOHANNES ASPMAN[†], JIŘÍ NĚMEČEK[†], AND JAKUB MAREČEK[†]

ABSTRACT. We consider approximating so-called tame functions, a class of nonsmooth, nonconvex functions, with piecewise polynomial functions. Tame functions appear in a wide range of applications: functions encountered in the training of deep neural networks with all common activations, value functions of mixed-integer programs, or wave functions of small molecules. We bound the quality of approximation of a tame function by a piecewise polynomial function with a given number of segments on any full-dimensional cube. We also present the first ever mixed-integer programming formulation of piecewise polynomial regression. Together, these can be used to estimate tame functions. We demonstrate promising computational results.

1. INTRODUCTION

In a wide range of applications, one encounters nonsmooth and nonconvex functions that are *tame*, short for *definable in o-minimal structures*. Such functions can be decomposed in a finite number of regions, where the function is smooth across each region, as illustrated in Fig. 1 (left pane). Tame functions appear in a broad range of useful and difficult, i.e., nonsmooth and nonconvex, applications. Prominent examples are all common (nonsmooth and nonconvex) deep learning architectures [7, 13], and (nonsmooth) empirical risk minimization frameworks [22]. Tame functions also appear, e.g., in mixed-integer optimization, with the value function and the solution to the so-called subadditive dual [2]; in quantum information theory, with approximations of the matrix exponential for a k -local Hamiltonian [1, 9]; and in quantum chemistry, with functions describing the electronic structure of molecules. The tame assumption was key in recent advances in learning theory, with notably the first convergence proofs of Stochastic Gradient Descent [5, 13, 14], or theory of automatic differentiation [7]. The tameness property of a function is, among other things, stable under composition. We will discuss these aspects in more detail later on.

This paper is concerned with building approximation of tame nonsmooth functions, a topic which has received attention recently [10, 16, 29]. Formally, given a function f , we seek a function p in a set of simple functions \mathcal{P} that minimizes the distance from p to f over a domain A :

$$\inf_{p \in \mathcal{P}} \left(\|f - p\|_{A, \infty} = \sup_{x \in A} |f(x) - p(x)| \right). \quad (1)$$

A major challenge is the nonsmoothness of the function to approximate. Classical polynomial approximation theory shows that good (“fast”) polynomial approximation of a function is possible if the function has a high degree of regularity. Specifically, if f is a function $(r + 1)$ -times continuously differentiable, the best degree n polynomial incurs an $\mathcal{O}(1/n^r)$ error [31]. However, the situation changes dramatically when the function has low regularity, e.g., is continuous but with discontinuous derivatives, as is the case for most settings in learning theory. Indeed, approximating the absolute value — the simplest

[†] FACULTY OF ELECTRICAL ENGINEERING, CZECH TECHNICAL UNIVERSITY OF PRAGUE, THE CZECH REPUBLIC.

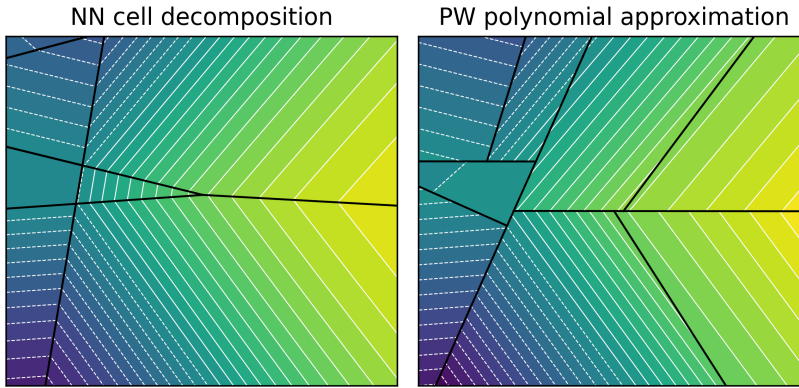


Figure 1: Left pane: a generic 2-dimensional function, with level lines (white) and nonsmooth points (black). Right pane: piecewise polynomial approximation of the network, obtained from the proposed integer program with a depth 3 regression tree and degree 2 polynomials.

nonsmooth function — by degree n polynomials over the interval $[-1, 1]$ incurs *exactly* the slow rate $1/n$:

$$\inf_{p \in \mathcal{P}_n} \|p - |\cdot|\|_{\infty, [-1, 1]} = \frac{\beta}{n} + o\left(\frac{1}{n}\right), \quad (2)$$

where $\beta \approx 0.28$ [3]. In sharp contrast, allowing approximation by *piecewise polynomials* makes this problem simpler: the absolute value itself is a piecewise polynomial, consisting of two polynomial pieces of degree 1. As a second example, consider the neural network displayed in Fig. 5, comprised of sigmoid, tanh, and ReLU activations. Its landscape contains nonsmooth points, showed in black in Fig. 1 (left pane). As the empirical risk minimization is tame, the nonsmooth points delineate regions of space where the function behaves smoothly. We know of no convergent method for finding a piecewise polynomial approximation of tame functions.

Related work. While simple, these examples illustrate the two fundamental challenges of estimating nonsmooth functions:

- (i) estimating the *cells* of the function, that is the full-dimensional sets on which the function is smooth; and,
- (ii) estimating the function on each cell.

These challenges require input from several branches of mathematics.

For (i), one can consult Model Theory, and, more specifically, o-minimal structures. Let us recall a central theorem there: the graph of any tame function splits into *finitely* many full-dimensional sets, known as “cells”, on which the function can have any desired degree of smoothness [35]. A natural approach is then to estimate this cell decomposition of the space. Rannou [32] reduces this to a quantifier elimination problem and proposes a procedure that takes doubly-exponential time, for semialgebraic functions. We are not aware of any implementation of this approach. Helmer & Nanda [19, 20] tested an implementation for real algebraic varieties and, possibly, semialgebraic sets. We propose an algorithm that applies to general tame functions, thus covering the semialgebraic case but also networks using e.g., sigmoid or tanh activations.

In Machine Learning, Hanin & Rolnick [18], Liu et al. [28], Serra et al. [33] study the cells of networks built from ReLU activation and linear layers. They provide bounds on the

number of cells, as well as a way to compute the cells of a given network by a mixed-integer linear program. In contrast, we propose to approximate the tame function by a piecewise polynomial function such that each piece is defined by affine inequalities. Thus, the whole domain is partitioned by a series of affine-hyperplane cuts, organized in a hierarchical tree structure, and a polynomial function is fit to each region.

To address (ii), Computational Statistics approximate smooth functions by polynomials on polytopes. There, algorithms are mostly focused on continuous and typically one-dimensional functions [17, 23, 37, 38], and often restricted to approximation of piecewise linear functions, [21, 25, 36]. Piecewise polynomial regression with polynomials of degree $n \geq 2$ is either not addressed [17, 37, 38] or done through “dimensionality lifting” by appending values of all monomials of degrees 2 to n as extra features to the individual samples [23]. This approach of Jekel & Venter [23] requires to know the nonsmooth points in advance. We make no such assumption.

In Machine Learning, the use of trees befits the task of piecewise polynomial regression, with regression in dimensions higher than 1 utilizing hierarchical partitioning of the input space. In Madrid Padilla et al. [29], the Dyadic CART algorithm of Donoho [16] is used to recover a piecewise constant function defined on a lattice of points on the plane, with typical application in image processing and denoising. This builds upon the work on Optimal Regression Trees (ORT) for classification by Bertsimas & Dunn [4], and is concerned with the optimal axis-aligned partitioning of the space, resulting in a piecewise constant function. We stress that Madrid Padilla et al. [29] only suggest a brute-force computation of the trees for piecewise constant functions.

In Statistical Theory, Chatterjee & Goswami [10] reasons about sample complexity of piecewise polynomial regression via ORT, which also assumes that the data is defined over a lattice and that the splits are axis-aligned, but accommodates fitting polynomials of arbitrary degree and lattices of points in arbitrary dimensions $d \geq 2$. The lattice data structure assumption facilitates the possibility of using dynamic programming to solve the mixed-integer program, leading to polynomial-time complexity in the number of samples n_{samp} , but has never been demonstrated in practice. Two obvious shortcomings of the above approaches are that they require both that the data be defined over a regular lattice and that the splits of the tree are axis-aligned. We know of no proposal to compute optimal regression trees without requiring axis-aligned splits. This significantly limits the type of piecewise polynomial functions they can reasonably fit, such as the neural network of Fig. 1, the example function (4) illustrated in Figure 2, or even the simple $\|\cdot\|_\infty$ polyhedral norm. Our contributions. In this work, we combine these results from model theory, approximation theory and optimization theory to present:

- the first theoretical bound on the approximation error of generic *nonsmooth and nonconvex* tame functions by piecewise polynomial functions, see Theorem 1;
- a procedure to compute the best piecewise polynomial function, where each piece is a polyhedron defined by a number of affine inequalities, and the polynomial on each piece has a given degree.

The latter procedure involves sampling the function, and then solving the mixed-integer optimization problem formulated in Eq. (19), which extends the OCT-H formulation of Bertsimas & Dunn [4] to the regression task. Specifically, we propose a new MIP formulation for finding provably optimal regression trees with arbitrary hyperplane splits and polynomials of arbitrary degree in the partitions. In other words, the method finds optimal piecewise polynomial functions in any dimension and for any degree polynomials, with hierarchical partitioning of the space. We find that such mixed-integer programs can be solved by current

solvers to global optimality with one hundred samples within one hour to global optimality to yield precise piecewise polynomial approximations with affine-hyperplane splits.

Figure 1 shows the output of the proposed procedure on a tame neural network involving sigmoid, tanh and ReLU activations. The left pane shows the level lines, and the nonsmooth points (in black) that constitute the boundaries of the cells on which the function is smooth. The right pane shows the approximation found using the formulation proposed in Section 4 after one hour of computation.

Notation. $\mathcal{C}^r(A)$ is the set of r times continuously differentiable functions from A to \mathbb{R} . For a function $f : A \rightarrow \mathbb{R}$, we define $\text{diff}_r(f)$ to be the subset of A such that all of the r -th order partial derivatives of f exists. For a real-valued function $f : A \rightarrow \mathbb{R}$ of a set A , we let $\|f\|_{\infty, A} \triangleq \sup_{x \in A} |f(x)|$. We drop the set A when it is clear from context. The diameter of a compact set $A \subset \mathbb{R}^d$ defines as $\text{diam}(A) = \sup_{x, y \in A} \|x - y\|$. $\text{cl}(A)$ denotes the closure of the set A . For any positive integer $n \in \mathbb{N}$, $[n]$ denotes the set of integers from 1 to n .

2. BACKGROUND ON TAME GEOMETRY

In this section we outline the main ideas and intuitions of tame geometry, and present the main result of interest: cell decomposition. A more formal presentation is deferred to Appendix A.

2.1. Definability in o-minimal structures. An o-minimal structure is a collection of certain subsets of \mathbb{R}^m that are stable under a large number of operations. One of the key properties that it should have is that when considering one-dimensional sets, they are only given by *finite* unions of intervals and points. The structure is furthermore closed under boolean operations, e.g. taking closures, unions or complements, as well as under projections to lower-dimensional sets, and elementary operations such as addition, multiplication and composition.

We use the words *definable* and *tame* interchangeably to refer to sets or functions that belong to a given o-minimal structure. Tame functions are in general nonsmooth and nonconvex, but the tameness properties still make it possible to have some control when studying the behaviour of these functions. The function class is also broad enough to entail most of the cases that would appear in applications in a vast number of fields. For example, in machine learning, most functions that would appear as activation functions in neural networks are tame.

Due to the balance between being wild enough to include a large number of non-trivial applications while still being tame enough such that it is possible to derive qualitative results on their behaviour, the interest in tame functions have seen a recent surge in numerous fields. In mathematical optimization, this framework allowed showing results that had proved elusive, notably on the convergence to critical points or escaping of saddle points for various (sub)gradient descent algorithms [5, 13, 24].

Example 1 (Analytic-exponential structure). Probably the most important o-minimal structure for applications is the one consisting of the analytic-exponential sets, which forms a structure typically denoted $\mathbb{R}_{\text{an}, \text{exp}}$. An *analytic-exponential set* in \mathbb{R}^d defines as a finite union of sets of the form

$$\{x \in \mathbb{R}^d : f_1(x) = 0, \dots, f_k(x) = 0, \\ g_1(x) > 0, \dots, g_l(x) > 0\}, \quad (3)$$

for some finite k, l , where the f_i and g_i are functions obtained from combinations of the following collections:

- i. coordinate functions $x \mapsto x_i$ and polynomial/semialgebraic functions,

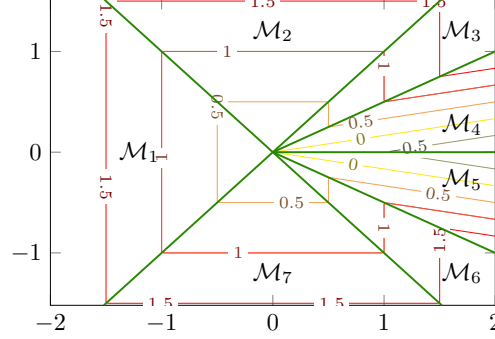


Figure 2: Illustration of the “cone” function (4), with $s^{\text{cone}} = r^{\text{cone}} = 0.5$, showing (i) the level lines of the function, and (ii) the decomposition of the domain into cells on which the function is smooth, as provided by Proposition 1; see Table 5 for details.

- ii. the restricted analytic functions: the functions $h : \mathbb{R}^d \rightarrow \mathbb{R}$ such that $h|_{[-1,1]^d}$ is analytic and h is identically zero outside $[-1,1]^d$,
- iii. the inverse function $x \mapsto 1/x$, with the convention that $1/0 = 0$,
- iv. and the real exponential and logarithm function (the latter is extended to \mathbb{R} by setting $\log(x) = 0$ for $x \leq 0$).

In particular, any function built from the above rules is definable in the structure $\mathbb{R}_{\text{an,exp}}$. Examples include almost all deep learning architectures, but also conic convex functions, wave functions of small molecules, or the following contrived functions $(x, y) \mapsto x^2 \exp(-\frac{y^2}{x^4+y^2})$, $(x, y) \mapsto x^{\sqrt{2}} \ln(\sin y)$ for $(x, y) \in (0, \infty) \times (0, \pi)$, or $(x, y) \mapsto y/\sin(x)$ for $x \in (0, \pi)$ [26, Sec. 1].

2.2. Tame functions are piecewise C^r . One of the central results in o-minimality theory is the cell decomposition theorem, and the related stratification theorems. These theorems give structural results on the graphs of tame functions by describing how the graph can be partitioned into smaller sets with some control on how the pieces fit together, as well as on the regularity of the function on each piece. In particular, it tells us that we can partition the graph into a finite number of pieces such that the function is C^r , for any $r < \infty$, on each piece. We introduce the result in a simplified form that best suits our needs. The more detailed statements are given in Appendix A.

Proposition 1 (C^r -cell decomposition). *Fix an o-minimal expansion of \mathbb{R} . Consider a definable full-dimensional set $A \subset \mathbb{R}^d$ and a definable function $f : A \rightarrow \mathbb{R}$. Then, for any positive integer r , there exists a finite collection \mathcal{W} of sets $\mathcal{M} \subset \mathbb{R}^d$, called cells, such that*

- each cell $\mathcal{M} \in \mathcal{W}$ is open, definable, full-dimensional,
- the sets of \mathcal{W} are pair-wise disjoint,
- A is the union of the closures of the elements of \mathcal{W} ,
- the restriction of f to each cell $\mathcal{M} \subseteq \mathcal{W}$ is C^r .

Proof. This proposition is a direct corollary of the cell decomposition theorem and the Whitney stratification theorem of definable maps, recalled in Appendix A, with \mathcal{W} corresponding to the set of all full-dimensional strata. ■

Example 2. Consider the following tame (piecewise linear) function of \mathbb{R}^2 :

$$f^{\text{cone}}(x) = \begin{cases} -s^{\text{cone}}x_1 + \frac{1+s^{\text{cone}}}{r^{\text{cone}}}x_2 & \text{if } x_1 > 0 \text{ and } 0 < x_2 < r^{\text{cone}}x_1 \\ -s^{\text{cone}}x_1 - \frac{1+s^{\text{cone}}}{r^{\text{cone}}}x_2 & \text{if } x_1 > 0 \text{ and } -r^{\text{cone}}x_1 < x_2 < 0 \\ \|x\|_\infty & \text{else} \end{cases} \quad (4)$$

When $r^{\text{cone}} = s^{\text{cone}} = 0.5$, as guaranteed by [Proposition 1](#), the domain of the function splits in 7 cells $(\mathcal{M}_i)_{i \in [7]}$, on which the function behaves smoothly. Here the pieces are polytopes, on which the function is linear. [Figure 2](#) shows the landscape of the function, and collection of cells $\mathcal{W} = (\mathcal{M}_i)_{i \in [7]}$. In addition, [Table 5](#) of [Appendix A](#) summarizes the analytic expressions of the cells and of the (smooth) restriction of the function on each cell.

3. APPROXIMATION OF TAME FUNCTIONS

In this section, we state our main theoretical result: any tame function can be approximated to an arbitrary precision by a piecewise polynomial function.

Definition 1 ((Piecewise) polynomial functions). We let \mathcal{P}_n denote the set of polynomials of degree at most n , and $\mathcal{P}_n^k(A)$ denote the set of functions that are piecewise polynomial on A , with

- (1) at most k pieces, each of which is a full-dimensional polyhedron, and
- (2) the restriction of the function to each piece is a polynomial of degree at most n .

We are now ready to state our main result, which combines the cell decomposition, [Proposition 1](#), with a more classical result from smooth function approximation theory.

Theorem 1 (Main result). *Consider a cubic set A , a function $f : A \rightarrow \mathbb{R}$, and a constant $K > 0$ such that:*

- *f is definable in an o-minimal structure, and*
- *f is K -Lipschitz on A : for all $x, y \in A$, $|f(x) - f(y)| \leq K\|x - y\|$.*

Then f is piecewise approximable by polynomials: for any integers $k \geq 1$, and $n \geq r > 1$, there holds

$$\inf_{p \in \mathcal{P}_n^k(A)} \|f - p\|_{\infty, A} \leq \max \left(\frac{C_1}{kn^{r-1}}, \frac{C_2}{k^{1/d}} \right), \quad (5)$$

where C_1 and C_2 are constants that depend on d, r, K, A , and the r -th derivative of f .

[Theorem 1](#) is our main approximation result so, before discussing its proof (which we carry out in detail in [Appendix B](#)), some remarks are in order.

We give expressions for the constants C_1 and C_2 that clarify their dependence to the parameters of the problem, see [Eq. \(B.13\)](#) in [Appendix B](#) for the detailed expressions.

The first term of the bound quantifies the approximation of f on regions of A where f is *smooth*. These regions correspond to the interior of the cells provided by [Proposition 1](#). This term goes to zero as the degree n of the polynomial approximation increases, or as the smoothness r of the underlying function increases. Notably, when f itself is polynomial on the cells and r is high enough, the term $C_1 \propto \|\frac{\partial^r f}{\partial x_j^r}\|_{\infty, \text{diff}_r(f)}$ vanishes and the polynomial approximant matches f exactly.

The second term of the bound quantifies the approximation of f on *nonsmooth* regions. This term goes to zero as the size of the pieces of the polynomial that contain nondifferentiability points of f goes to zero. This is ensured by increasing the number of pieces k .

Table 1: Summary of the hyperparameters

parameter	interpretation
D	depth of the binary tree
N_{min}	minimal number of points allowed in a nonempty leaf
n	maximum degree of the polynomial on each piece

Proof outline of [Theorem 1](#). The bound is obtained by considering polynomials of $\mathcal{P}_n^k(A)$ such that their pieces are obtained by regularly slicing the domain $L = \lfloor k^{1/d} \rfloor$ times along each cartesian axis, leading to a partition of A in L^d regular small cubes. The problem then reduces to finding the best degree n polynomial approximation of f on each of the small slices. Either (i) f is smooth on the given slice, in which case classical results of smooth approximation theory (e.g., Jackson’s theorem) provides a good degree r polynomial approximation and a corresponding bound on the error, or (ii) f is nonsmooth on the slice. In that case, as discussed in the introduction, high degree polynomials provide poor approximations. We thus use a well-suited linear approximation, along with the Lipschitz property of the function.

Remark 1 (Extensions to non-cubic domains). The domain A on which f is approximated is a full-dimensional cube. However, one might use approximation of smooth multivariate functions on more general domains, e.g., polyhedral or more general [\[12, 34\]](#).

Remark 2. Our proof technique uses a regular partition of the approximation domain. It would be interesting to see if partitions of the domain adapted to the cell decomposition, i.e., that approximate the boundaries between the cells, would improve on the bound of [Theorem 1](#). Such adapted partitions are constructed in e.g., Boissonnat et al. [\[6\]](#).

4. MIXED-INTEGER FORMULATION OF PIECEWISE POLYNOMIAL APPROXIMATION

In this section, we formulate the problem of piecewise polynomial regression as a mixed-integer program (MIP), inspired by the optimal classification trees framework [\[4\]](#).

4.1. Mixed-integer formulation. The mixed-integer optimization problem expects as input n_{samp} points $(x_i)_{i=1}^{n_{\text{samp}}}$ that belong to A , and the corresponding function values $y_i = f(x_i)$ for $i = 1, \dots, n_{\text{samp}}$. Without loss of generality, we assume that the sample points belong to $[0, 1]^d$. The output is a piecewise polynomial function; the boundaries of the smooth pieces are defined by affine hyperplanes. [Tables 1 and 2](#) summarize the hyperparameters and variables of the mixed-integer formulation; we now explain the formulation details.

Binary tree. We consider a fixed binary tree of depth D . The tree has $T = 2^{D+1} - 1$ nodes, indexed by $t = 1, \dots, T$ such that all branching nodes are indexed by $t = 1, \dots, 2^D - 1$ and leaf nodes are indexed by $t = 2^D, \dots, 2^{D+1} - 1$. The sets of branching nodes and leaf nodes are denoted \mathcal{T}_B and \mathcal{T}_L respectively. Besides, the set of ancestors of node t is denoted $A(t)$. This set partitions in $A_L(t)$ and $A_R(t)$, the subsets of ancestors at which branching was performed on the left and right respectively. [Figure 3](#) shows a tree of depth $D = 2$ and illustrates these notions.

Affine-hyperplane partition of the space. At each branching node $m \in \mathcal{T}_B$, a hyperplane splits the space in two subspaces

$$a_m^\top x_i - b_m < 0 \quad a_m^\top x_i - b_m \geq 0, \quad (6)$$

that will be associated to the left and right children of node m . The parameters $a_m \in \mathbb{R}^d$ and $b_m \in \mathbb{R}$ are variables of the mixed integer program.

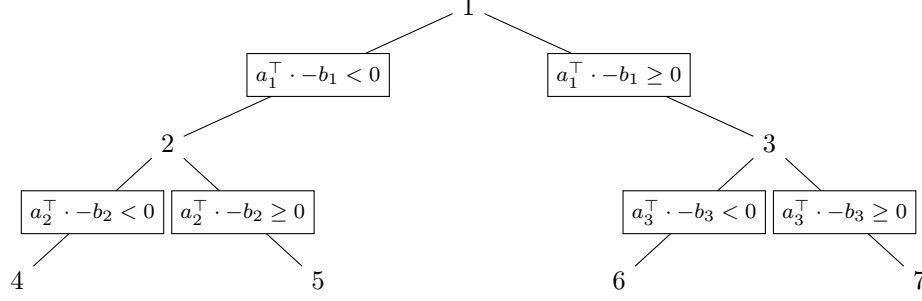


Figure 3: Binary tree structure and partition of the space. The ancestors of node 6 are $A(6) = \{1, 3\}$, and left and right branching ancestors are $A_L = \{3\}$ and $A_R = \{1\}$. To each leaf is associated an element of the partition, defined by the inequalities of its ancestors. The set corresponding to leaf 6 is $\{x \in \mathbb{R}^d : a_1^\top x \geq b_1, a_3^\top x < b_3\}$.

Table 2: Summary of the variables of the affine-hyperplane regression tree formulation

variable	index domain	interpretation
$l_t \in \{0, 1\}$	$t \in \mathcal{T}_L$	1 iff any point is assigned to leaf t
$z_{it} \in \{0, 1\}$	$t \in \mathcal{T}_L, i \in [n_{\text{samp}}]$	1 iff point x_i is assigned to leaf t
$a_m \in \mathbb{R}^d$	$m \in \mathcal{T}_B$	coefficients of the affine cut
$b_m \in \mathbb{R}$		
$o_{jm} \in \{0, 1\}$	$m \in \mathcal{T}_B, j \in [d]$	1 iff coordinate j of a_m is positive
$a_m^+, a_m^- \in \mathbb{R}$	$m \in \mathcal{T}_B$	the positive and negative part of a_m
$\phi_{it} \in \mathbb{R}$	$t \in \mathcal{T}_L, i \in [n_{\text{samp}}]$	fit error of point x_i by the polynomial of leaf t
$\delta_i \in \mathbb{R}$	$i \in [n_{\text{samp}}]$	fit error of point x_i by the piecewise polynomial function
$c_t \in \mathbb{R}^{\binom{n+d-1}{d-1}}$	$t \in \mathcal{T}_L$	coefficients of the degree n polynomial associated with leaf t

Making this formulation practical requires two precisions. First, in order to avoid scaling issues, we constrain a_m to belong in $[-1, 1]^d$, such that $\|a_m\|_1 = 1$.¹ This formulates as

$$\sum_{j=1}^d (a_{jt}^+ + a_{jt}^-) = 1 \quad (7)$$

$$a_{jt} = a_{jt}^+ - a_{jt}^- \quad \forall j \in [d] \quad (8)$$

$$a_{jt}^+ \leq o_{jt} \quad \forall j \in [d] \quad (9)$$

$$a_{jt}^- \leq (1 - o_{jt}) \quad \forall j \in [d] \quad (10)$$

Furthermore, since $x_i \in [0, 1]$, it holds that $a_m^\top x_i \in [-1, 1]$, so that b_m is constrained to $[0, 1]$ without loss of generality. Second, we implement the strict inequality (6) by introducing variable z_{it} and a small constant $\mu > 0$. Noting that $a_t^\top x_i - b_t$ takes values in the interval $[-2, 2]$, the affine split inequalities (6) now formulate as

$$a_m^\top x_i \geq b_m - 2(1 - z_{it}) \quad \forall m \in A_R(t) \quad (11)$$

$$a_m^\top x_i + \mu \leq b_m + (2 + \mu)(1 - z_{it}) \quad \forall m \in A_L(t) \quad (12)$$

both for all i in $[n_{\text{samp}}]$ and all t in \mathcal{T}_L .

¹We depart here from the OCT-H formulation of [4], which constrains the norm of a_m to be at most 1.

Regression on each partition element. Each leaf $t \in \mathcal{T}_L$ corresponds to one element of the partition of A defined by the tree, and is associated with a degree r polynomial $\text{poly}(\cdot; c_t)$ whose coefficients are parameterized by variable c_t . The regression error of point x_i by the polynomial associated with leaf t is then

$$\phi_{it} = y_i - \text{poly}(x_i; c_t). \quad (13)$$

Each point x_i is assigned to a unique leaf of the tree: for all $i \in [n_{\text{samp}}]$,

$$\sum_{t \in \mathcal{T}_L} z_{it} = 1. \quad (14)$$

Furthermore, each leaf $t \in \mathcal{T}_L$ is either assigned zero or at least N_{\min} points:

$$\sum_{i=1}^{n_{\text{samp}}} z_{it} \geq N_{\min} l_t \quad \text{and} \quad z_{it} \leq l_t \quad \text{for all } i \in [n_{\text{samp}}]. \quad (15)$$

Minimizing the regression error. The objective is minimizing the average prediction error $\sum_{i=1}^{n_{\text{samp}}} |y_i - \text{poly}(x_i; c_{t(i)})|$, where $c_{t(i)}$ is the polynomial coefficients corresponding to the leaf to which x_i belongs. We formulate this as minimizing

$$\frac{1}{n_{\text{samp}}} \sum_{i=1}^{n_{\text{samp}}} \delta_i, \quad (16)$$

where δ_i models the absolute value of the prediction error for point x_i :

$$\delta_i \geq \phi_{it} - (1 - z_{it})M \quad \text{for all } t \in \mathcal{T}_L \quad (17)$$

$$\delta_i \geq -\phi_{it} - (1 - z_{it})M \quad \text{for all } t \in \mathcal{T}_L \quad (18)$$

where M is a big constant that makes the constraint inactive when $z_{it} = 0$. Note that the above big- M formulation can be replaced by indicator constraints, if the solver supports them, to encode that if $z_{it} = 1$, then $\delta_i \geq \phi_{it}$, $\delta_i \geq -\phi_{it}$. We further note that, the formulation could be changed to optimize the mean squared error, by changing the objective function to $n_{\text{samp}}^{-1} \sum_{i=1}^{n_{\text{samp}}} \delta_i^2$.

Combining these elements yields the affine hyperplane formulation:

$$\min \frac{1}{n_{\text{samp}}} \sum_{i=1}^{n_{\text{samp}}} \delta_i \quad (19a)$$

$$\text{s.t. } \delta_i \geq \phi_{it} - (1 - z_{it})M \quad \forall i \in [n_{\text{samp}}], \quad \forall t \in \mathcal{T}_L \quad (19b)$$

$$\delta_i \geq -\phi_{it} - (1 - z_{it})M \quad \forall i \in [n_{\text{samp}}], \quad \forall t \in \mathcal{T}_L \quad (19c)$$

$$\phi_{it} = y_i - \text{poly}(x_i; c_t) \quad \forall i \in [n_{\text{samp}}], \quad \forall t \in \mathcal{T}_L \quad (19d)$$

$$a_m^\top x_i \geq b_m - 2(1 - z_{it}) \quad \forall i \in [n_{\text{samp}}], \quad \forall t \in \mathcal{T}_L, \quad \forall m \in A_R(t) \quad (19e)$$

$$a_m^\top x_i + \mu \leq b_m + (2 + \mu)(1 - z_{it}) \quad \forall i \in [n_{\text{samp}}], \quad \forall t \in \mathcal{T}_L, \quad \forall m \in A_L(t) \quad (19f)$$

$$\sum_{t \in \mathcal{T}_L} z_{it} = 1 \quad \forall i \in [n_{\text{samp}}] \quad (19g)$$

$$z_{it} \leq l_t \quad \forall i \in [n_{\text{samp}}], \quad \forall t \in \mathcal{T}_L \quad (19h)$$

$$\sum_{i=1}^{n_{\text{samp}}} z_{it} \geq N_{\min} l_t \quad \forall t \in \mathcal{T}_L \quad (19i)$$

$$\sum_{j=1}^d (a_{jt}^+ + a_{jt}^-) = 1 \quad \forall t \in \mathcal{T}_B \quad (19j)$$

$$a_{jt} = a_{jt}^+ - a_{jt}^- \quad \forall j \in [d], \quad \forall t \in \mathcal{T}_B \quad (19k)$$

$$a_{jt}^+ \leq o_{jt} \quad \forall j \in [d], \quad \forall t \in \mathcal{T}_B \quad (19l)$$

$$a_{jt}^- \leq (1 - o_{jt}) \quad \forall j \in [d], \quad \forall t \in \mathcal{T}_B \quad (19m)$$

$$z_{it}, l_t \in \{0, 1\} \quad \forall i \in [n_{\text{samp}}], \quad \forall t \in \mathcal{T}_L \quad (19n)$$

$$o_{jt} \in \{0, 1\} \quad \forall j \in [d], \quad \forall t \in \mathcal{T}_B \quad (19o)$$

$$a_{jt}, b_t \in [-1, 1] \quad \forall j \in [d], \quad \forall t \in \mathcal{T}_B \quad (19p)$$

$$a_{jt}^+, a_{jt}^- \in [0, 1] \quad \forall j \in [d], \quad \forall t \in \mathcal{T}_B \quad (19q)$$

$$\phi_{it} \in \mathbb{R} \quad \forall i \in [n_{\text{samp}}], \quad \forall t \in \mathcal{T}_L \quad (19r)$$

The constraints Eqs. (19e)–(19i) are the optimal classification tree with hyperplanes (OCT-H) of Bertsimas & Dunn [4]; the other constraints are our extension thereof.

Remark 3 (Axis-aligned regression). In Appendix C, we propose a version of (19) tailored to functions whose cells have boundaries aligned with cartesian axes. Such functions appear in signal processing applications, and are the topic of recent works Bertsimas & Dunn [4], Chatterjee & Goswami [10], Madrid Padilla et al. [29].

5. NUMERICAL EXPERIMENTS

In this section, we demonstrate the applicability of the piecewise polynomial regression method developed in Section 4. Appendix D contains complementary details and experiments. Setup. We implement the affine-hyperplane formulation, detailed in Eq. (19), in Python and use Gurobi as the MIP solver. We present three applications: regression of the cone function (4), regression of a Neural Network, and denoising of a piecewise constant 2d signal, following the experiments of [29]. We use trees of varying depth $D \in \{2, 3, 4\}$ and polynomial degree $n \in \{0, 1, 2\}$. We set $N_{\min} = 1$ and $\mu = 10^{-4}$ across all experiments, and run experiments on a personal laptop.

5.1. Regression of tame functions. We consider the regression problem for two tame functions and report in Fig. 4 the level lines of the original function and the level lines of the piecewise polynomial approximations provided by the affine-hyperplane formulation (19). Quantitative error measures are reported in Table 3.

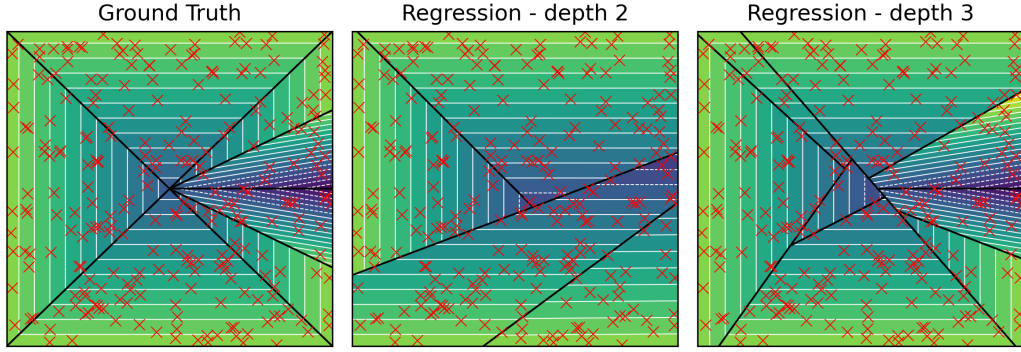
Piecewise-affine function. Firstly, we return to the “cone” function, introduced in (4).

$$f^{\text{cone}}(x) = \begin{cases} -s^{\text{cone}}x_1 + \frac{1+s^{\text{cone}}}{r^{\text{cone}}}x_2 & \text{if } x_1 > 0 \text{ and } 0 < x_2 < r^{\text{cone}}x_1 \\ -s^{\text{cone}}x_1 - \frac{1+s^{\text{cone}}}{r^{\text{cone}}}x_2 & \text{if } x_1 > 0 \text{ and } -r^{\text{cone}}x_1 < x_2 < 0 \\ \|x\|_\infty & \text{else} \end{cases} \quad (20)$$

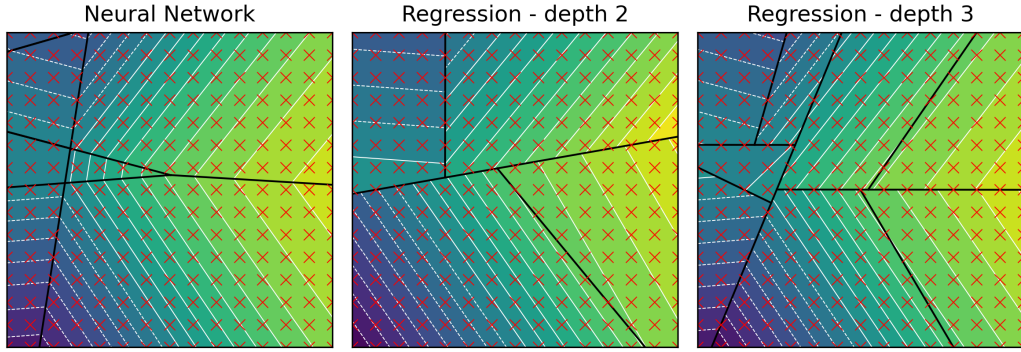
This function is piecewise-linear and continuous; see Fig. 4a (left pane) for an illustration. This is a nonconvex function for which estimating the correct full-dimensional cells with a sampling scheme gets harder as r^{cone} goes to zero or as the dimension of the space d increases.

Figure 4a (middle and right pane) shows the obtained piecewise approximation of f^{cone} (with $r^{\text{cone}} = s^{\text{cone}} = 0.5$), for depth 2 and 3 approximation trees with time budget of 5 and 10 minutes. There are $n_{\text{samp}} = 250$ points sampled uniformly; the polynomial degree is $n = 1$. The depth $D = 2$ tree fails to recover an approximation of the cells, as it can only approximate 4 cells while f^{cone} has 7 cells. The depth $D = 3$ recovers the cell decomposition well qualitatively, and reduces the error measures by a factor 2; see Table 3.

Non-piecewise-linear Neural Network. We consider a small neural network, comprised of 27 parameters, sigmoid, tanh, ReLU activations, and 1d max-pooling; see the architecture in Figure 5.



(a) The cone function (20).



(b) The neural network from Fig. 5

Figure 4: Tame functions and regression results for trees of depth 2 and 3. Red crosses are the coordinates of samples used for the training. Black lines show the decomposition of the space.

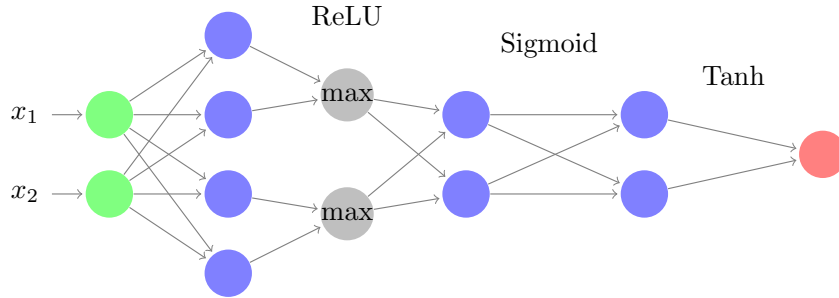


Figure 5: The architecture of the example Neural Network. Input neurons are green, blue nodes are neurons in hidden layers, and the output neuron is red. Grey nodes represent the max-pooling layer. Above the connections are the names of activation functions used on the outputs of the layer to the left of each respective name.

The neural network is trained to approximate the 2d function $x \mapsto 2 \sin x_1 + 2 \cos x_2 + x_2/2$, from 15 random samples on the cube $[-2, 2]^2$. The loss is the mean squared error over the 15 samples; it is optimized in a single batch for 5000 epochs using the **AdamW** algorithm.

Table 3: Normalized absolute error between tame functions and their approximations by the affine-hyperplane tree (19) of a given depth. The error is computed on a 1000×1000 grid of regularly spaced points. We divide the absolute errors by the maximal absolute value of the underlying ground truth.

Function	depth	max. err.	mean err.	median err.
f^{cone} (20)	2	5.0×10^{-1}	4.7×10^{-2}	1.0×10^{-4}
	3	3.7×10^{-1}	1.0×10^{-2}	6.4×10^{-5}
NN	2	3.3×10^{-1}	3.6×10^{-2}	2.5×10^{-2}
	3	1.9×10^{-1}	1.3×10^{-2}	9.3×10^{-3}

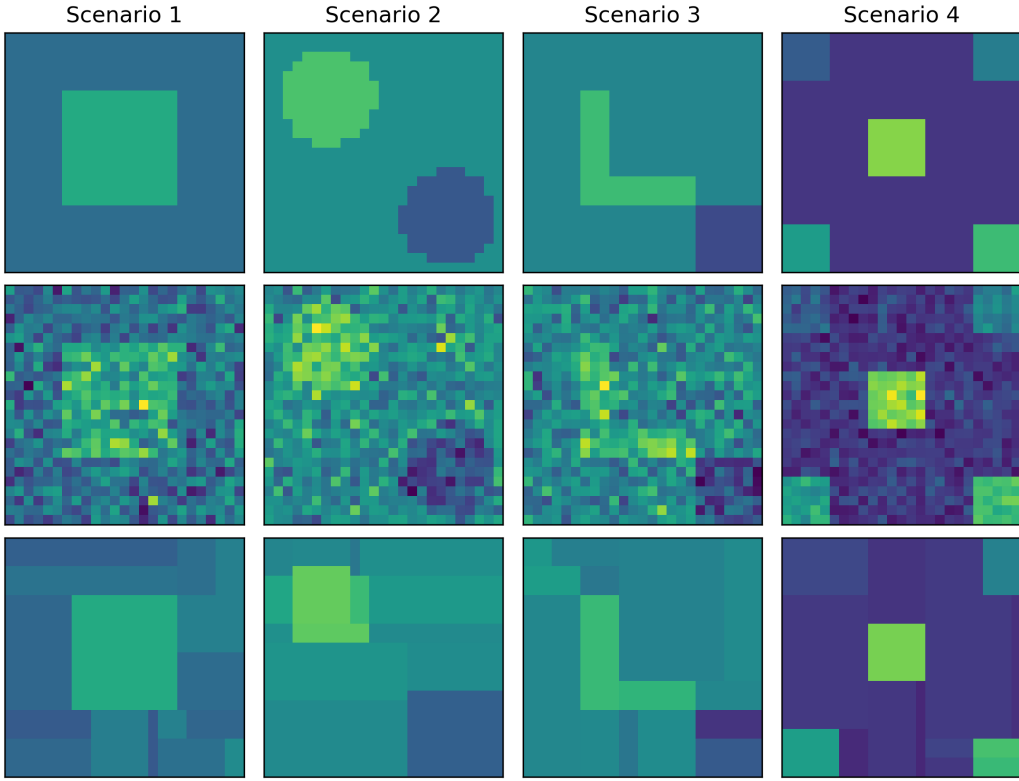


Figure 6: Four denoising scenarios from Madrid Padilla et al. [29, Figure 3]. The regression trees are restricted to axis-aligned splits and have depth 4. First row: ground truth, second row: (corrupted) regression signal, third row: recovered signal from the mixed integer formulation.

We approximate the output of the trained NN by taking $n_{\text{samp}} = 225 = 15^2$ points in a 15×15 regular grid over the approximation space and optimize the trees using that as input. We set the polynomial degree $n = 2$.

Figure 4b (middle and right pane) shows the obtained piecewise approximation of the Neural Network, for depth 2 and 3 approximation trees with time budget of 30 and 60 minutes. Increasing the depth from 2 to 3 reduces again the error measures by a factor of 2; see Table 3.

Table 4: Normalized absolute error for the denoising scenarios in Figure 6. The error is computed as the absolute difference between the ground truth signal and its approximation by the *axis-aligned* trees, divided by the maximal value of the ground truth.

Denoising	max. err.	mean err.	median err.
Scenario 1	1.1	1.4×10^{-1}	9.3×10^{-2}
Scenario 2	1.5	1.8×10^{-1}	9.0×10^{-2}
Scenario 3	9.5×10^{-1}	1.2×10^{-1}	5.5×10^{-2}
Scenario 4	8.3×10^{-1}	4.1×10^{-2}	1.6×10^{-2}

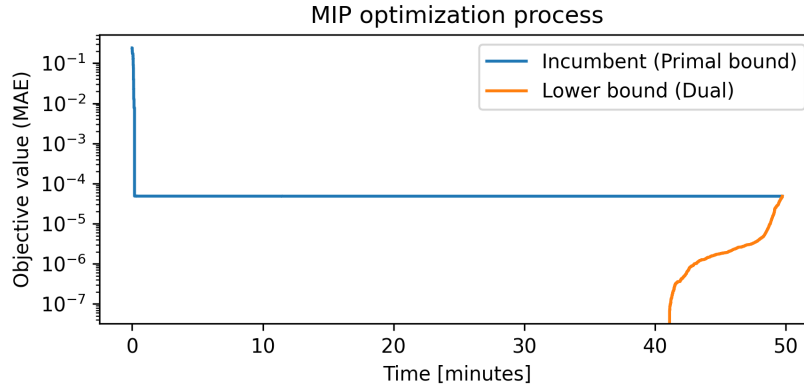


Figure 7: Objective value (mean absolute error) of the incumbent solution during the optimization. The full optimization takes 50 minutes, although a solution with almost optimal error is found within seconds.

5.2. Denoising of a piecewise-constant 2d signal. We consider now a slightly different set-up: following Madrid Padilla et al. [29], we consider four two-dimensional functions that are piecewise constant on a 25 by 25 grid, illustrated in Figure 6 (row one). The regression data is the function corrupted by an additive Gaussian with zero mean and standard deviation of $\sigma = 0.5$, illustrated in Figure 6 (row two). Row three of Figure 6 shows, for each scenario, the output of regression trees with depth $D = 4$ and polynomial degree $n = 0$, with a time limit of 1 hour.

The piecewise polynomial formulation used here is a simplified version of Eq. (19), where the splits are constrained to be aligned with the cartesian axes; see Appendix C for details.

Table 4 shows the recovery error of the regression trees; the recovered signals are comparable in quality to Figure 3 in Madrid Padilla et al. [29].

5.3. Notes on the optimization process. To study the MIP optimization process until completion, we choose the $\|\cdot\|_\infty$ norm. This is as a simple example of a tame function with partitions unfit for approximation by trees with axis-aligned splits, as in e.g., the recent works of Chatterjee & Goswami [10], Madrid Padilla et al. [29].

We optimize over $n_{\text{samp}} = 100$ randomly sampled points with depth $D = 2$ and polynomial degree $n = 1$. Figure 7 shows the evolution of objective value bounds: the blue curve shows the objective value of the best candidate found by the solver so far, the orange curve shows the best lower bound on the optimal objective value found so far. A candidate piecewise

polynomial function is proved to be optimal when the two curves coincide. Here, the mixed-integer solver takes almost 50 minutes to find a candidate piecewise polynomial function *and* prove its optimality. But already after 11 seconds, the candidate function has an objective value within 10^{-6} of the optimal objective value. Most of the effort in solving (19) is thus spent on proving optimality of the candidate function. This is an even more extreme contrast between the optimization of the two bounds as compared to the results for OCT [4].

This suggests that although the rest of our results were not proven optimal, the solutions could be close to optimal after a short computing time. Improvements in the search for lower (dual) bounds could be an important direction of future work.

APPENDIX A. TAME GEOMETRY

We give a more formal but brief review of the results needed from tame, or o-minimal, geometry. We refer the interested reader to Coste [11], Van den Dries [35] for extensive expositions.

Let us start with the definition of an o-minimal structure. For simplicity, we consider only structures over the real field \mathbb{R} .

Definition 2 (o-minimal structure). An o-minimal structure on \mathbb{R} is a sequence $\mathcal{S} = (\mathcal{S}_m)_{m \in \mathbb{N}}$ such that for each $m \geq 1$:

- i. \mathcal{S}_m is a boolean algebra of subsets of \mathbb{R}^m ;
- ii. if $A \in \mathcal{S}_m$, then $\mathbb{R} \times A$ and $A \times \mathbb{R}$ belongs to \mathcal{S}_{m+1} ;
- iii. $\{(x_1, \dots, x_m) \in \mathbb{R}^m : x_1 = x_m\} \in \mathcal{S}_m$;
- iv. if $A \in \mathcal{S}_{m+1}$, and $\pi : \mathbb{R}^{m+1} \rightarrow \mathbb{R}^m$ is the projection map on the first m coordinates, then $\pi(A) \in \mathcal{S}_m$;
- v. the sets in \mathcal{S}_1 are exactly the finite unions of intervals and points.

A set $A \subseteq \mathbb{R}^m$ is said to be *definable* in \mathcal{S} if A belongs to \mathcal{S}_m . Similarly, a map $f : A \rightarrow B$, with $A \subseteq \mathbb{R}^m$, $B \subseteq \mathbb{R}^n$, is said to be definable in \mathcal{S} if its graph $\Gamma(f) := \{(x, f(x)) \in \mathbb{R}^{m+n} : x \in A\}$ belongs to \mathcal{S}_{m+n} .

A set or function definable in some o-minimal structure is often simply referred to as *tame* when the specific o-minimal structure is not important.

The most fundamental o-minimal structure is that containing the semialgebraic sets:

Example 3 (Semialgebraic structure). A *semialgebraic set* in \mathbb{R}^d defines as a finite union of sets of the form

$$\{x \in \mathbb{R}^d : f_1(x) = 0, \dots, f_k(x) = 0, g_1(x) > 0, \dots, g_l(x) > 0\} \quad (\text{A.1})$$

where the f_i and the g_i are all real polynomials in d variables.

The collection of all semialgebraic sets forms an o-minimal structure. In particular, any function built from polynomials, boolean rules, and coordinate projections is definable in that structure. Examples include affine applications, piecewise polynomial functions such as linear layers, (pointwise) ReLU activation functions, and their composition, or functions such as $(x, y) \mapsto \sqrt{x^2 + y^3}$.

As stated in Proposition 1, tame sets can always be partitioned into smaller subsets. For completeness, we state the formal cell decomposition theorem. To this end, we first need the following.

Definition 3 (Cells, decompositions). We define both cells and decompositions inductively. A *cell* in \mathbb{R} is a point $\{a\}$, for $a \in \mathbb{R}$ or an (open) interval (a, b) , for $a, b \in \mathbb{R} \cup \{\pm\infty\}$.

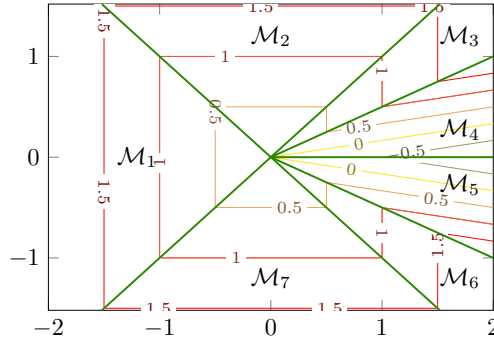


Figure 8: Illustration of the “cone” function (4), with $s^{\text{cone}} = r^{\text{cone}} = 0.5$, showing (i) the level lines of the function, and (ii) the decomposition of the domain into cells on which the function is smooth, as provided by Proposition 1; see Table 5 for details.

- Let C be a cell in \mathbb{R}^m and let $f : C \rightarrow \mathbb{R}$ be tame and continuous, then $\{(x, f(x)) : x \in C\}$ is a cell in \mathbb{R}^{m+1} .
- Let C be a cell in \mathbb{R}^m and let $f, g : C \rightarrow \mathbb{R} \cup \{\pm\infty\}$ be tame and continuous such that for all $x \in C$: $f(x) < g(x)$, then $\{(x, y) \in C \times \mathbb{R} : f(x) < y < g(x)\}$ is a cell in \mathbb{R}^{m+1} .

A *decomposition* of \mathbb{R} is a finite partition of the form

$$\{(-\infty, a_1), (a_1, a_2), \dots, (a_n, +\infty), \{a_1\}, \dots, \{a_n\}\}, \quad (\text{A.2})$$

and a decomposition of \mathbb{R}^{m+1} is a finite partition of \mathbb{R}^{m+1} into cells C_1, \dots, C_n such that the set of projections $\pi(C_j)$ gives a partition of \mathbb{R}^m .

Cells are connected sets. We further say that a cell is C^r if all functions used to construct the cell are C^r . We now have the fundamental result:

Theorem A.1 (Cell decomposition, cf. Thm. 7.3.2 [35]). *For any definable sets $A, A_1, \dots, A_n \subseteq \mathbb{R}^m$ and definable function $f : A \rightarrow \mathbb{R}$, there is*

- a decomposition of \mathbb{R}^m into C^r -cells partitioning the sets A_j .
- a decomposition of \mathbb{R}^m into C^r -cells partitioning A , such that each restriction $f|_C : C \rightarrow \mathbb{R}$ is C^r for each cell $C \subseteq A$ of the decomposition.

Example 4 (Example 2 continued). We return on the cone function, defined in Eq. (4) as

$$f(x) = \begin{cases} -s^{\text{cone}}x_1 + \frac{1+s^{\text{cone}}}{r^{\text{cone}}}x_2 & \text{if } x_1 > 0 \text{ and } 0 < x_2 < r^{\text{cone}}x_1 \\ -s^{\text{cone}}x_1 - \frac{1+s^{\text{cone}}}{r^{\text{cone}}}x_2 & \text{if } x_1 > 0 \text{ and } -r^{\text{cone}}x_1 < x_2 < 0 \\ \|x\|_\infty & \text{else} \end{cases} \quad (\text{A.3})$$

The above cell decomposition theorem provides the cells described in Table 5; see Fig. 8 for an illustration.

A related notion to that of cell decomposition is that of stratifications. A stratification is slightly stronger than a cell decomposition, in that it gives further conditions on how the different pieces fit together. The basic idea is that the set is partitioned into a finite number of manifolds, called the *strata*, with some additional conditions on how the different strata glue together. Various types of stratifications, with differing conditions on the gluing of the strata, exist in the literature. Some examples are the Whitney, Verdier and Lipschitz conditions; see e.g., Lê Loi [27]. For o-minimal structures, we can again require that the

Table 5: Cell decomposition of the “cone” function (4) with $r^{\text{cone}} = s^{\text{cone}} = 0.5$: the space decomposes in 7 open full-dimensional sets on which the function is smooth; see Fig. 2 for an illustration.

Cell	cell expression	f restricted to cell
\mathcal{M}_1	$\{x \in \mathbb{R}^2 : x_1 + x_2 < 0, x_1 - x_2 < 0\}$	$f _{\mathcal{M}_1} = -x_1$
\mathcal{M}_2	$\{x \in \mathbb{R}^2 : x_1 + x_2 < 0, x_1 - x_2 > 0\}$	$f _{\mathcal{M}_2} = x_2$
\mathcal{M}_3	$\{x \in \mathbb{R}^2 : x_1 + x_2 > 0, x_1 - x_2 > 0\}$	$f _{\mathcal{M}_3} = x_1$
\mathcal{M}_4	$\{x \in \mathbb{R}^2 : x_1 > 0, 0 < x_2 < 0.5x_1\}$	$f _{\mathcal{M}_4} = -0.5x_1 + 3x_2$
\mathcal{M}_5	$\{x \in \mathbb{R}^2 : x_1 > 0, 0 < -x_2 < 0.5x_1\}$	$f _{\mathcal{M}_5} = -0.5x_1 - 3x_2$
\mathcal{M}_6	$\{x \in \mathbb{R}^2 : x_1 + x_2 > 0, x_1 - x_2 < 0\}$	$f _{\mathcal{M}_6} = x_1$
\mathcal{M}_7	$\{x \in \mathbb{R}^2 : x_1 + x_2 < 0, x_1 - x_2 < 0\}$	$f _{\mathcal{M}_7} = -x_2$

function is \mathcal{C}^r , for some $r < \infty$, on each strata. The additional gluing conditions have played a vital role in the recent optimization literature when addressing e.g., questions of convergence for gradient descent algorithms to Clarke critical points [8, 13, 14].

APPENDIX B. PROOF OF THEOREM 1

We recall Theorem 1:

Theorem 1 (Main result). *Consider a cubic set A , a function $f : A \rightarrow \mathbb{R}$, and a constant $K > 0$ such that:*

- f is definable in an o-minimal structure, and
- f is K -Lipschitz on A : for all $x, y \in A$, $|f(x) - f(y)| \leq K\|x - y\|$.

Then f is piecewise approximable by polynomials: for any integers $k \geq 1$, and $n \geq r > 1$, there holds

$$\inf_{p \in \mathcal{P}_n^k(A)} \|f - p\|_{\infty, A} \leq \max \left(\frac{C_1}{kn^{r-1}}, \frac{C_2}{k^{1/d}} \right), \quad (5)$$

where C_1 and C_2 are constants that depend on d, r, K, A , and the r -th derivative of f .

Theorem 1 will follow from a slightly more general result. Let $\tilde{\mathcal{P}}_n^l(A)$ denote the set of piecewise polynomial functions such that (i) the cells of the function form a hierarchical partition of A of depth l , and (ii) the polynomial on each piece has degree at most n . This is exactly the class of piecewise polynomial functions modelled by the mixed-integer formulation of Section 4. This result gives an upper bound on the approximation error of a tame function by polynomials in that function class.

Theorem B.1. *Consider a cubic set A , a function $f : A \rightarrow \mathbb{R}$, and a constant $K > 0$ such that:*

- f is definable in an o-minimal structure, and
- f is K -Lipschitz on A : for all $x, y \in A$, $|f(x) - f(y)| \leq K\|x - y\|$.

Then f is piecewise approximable by polynomials: for any integers $l \geq 1$, and $n \geq r > 1$, there holds

$$\inf_{p \in \tilde{\mathcal{P}}_n^l(A)} \|f - p\|_{\infty, A} \leq \max \left(\frac{C'_1}{l^d n^{r-1}}, \frac{C'_2}{l} \right), \quad (\text{B.1})$$

where $C'_1 = d^d \text{diam}(A)^d C_{d,r} \sum_{j=1}^d \left\| \frac{\partial^r f}{\partial x_j^r} \right\|_{\infty, \text{diff}_r(f)}$ and $C'_2 = dK \text{diam}(A)$.

Before proceeding to the proof of [Theorem B.1](#), we recall a result from approximation of C^r functions on a cube mentioned in Pleśniak [\[31\]](#).

Proposition B.1 (Multivariate Jackson theorem). *Let X be a compact cube in \mathbb{R}^d , $f : X \rightarrow \mathbb{R}$ a $C^r(X)$ function, and $n \geq r$ two integers. Then there exists a constant $C_{d,r}$ depending only on d , and r such that:*

$$\inf_{p \in \mathcal{P}_n(X)} \|f - p\|_{\infty, X} \leq \text{diam}(X)^d \frac{C_{d,r}}{n^{r-1}} \sum_{j=1}^d \left\| \frac{\partial^r f}{\partial x_j^r} \right\|_{\infty, X}, \quad (\text{B.2})$$

where $\text{diam}(X)$ denotes the edge length of X .

Proof of Proposition B.1. This result is obtained by reproducing the steps of Proposition 2.4 of Pleśniak [\[30\]](#), specializing to a cube which edge have same length $\text{diam}(X)$, and tracking the dependency in the size of the cube when combining Theorem 2.1 and Lemma 2.2 in Pleśniak [\[30\]](#). ■

Remark 1. We are not aware of a similar results in prominent approximation theory literature [\[12, 15, 34\]](#) that propose an approximation result on a cubic domain, in which the constant C is independent of the geometry of the domain. This last point is essential for our purposes, since this result will be applied to small domains the size of which depends on parameters n and k of [Theorem 1](#).

We now proceed with the proof of [Theorem B.1](#).

Proof of Theorem B.1. Consider the set \mathcal{C}_p of closed cubes obtained by regularly slicing the approximation domain $L \triangleq \lfloor l/d \rfloor + 1$ times along each cartesian axis. The domain A is thus split in $k = L^d$ pieces, each of which is a cube of edge length $\text{diam}(A)/L$. Consider the set \mathcal{P}_L of functions from A to \mathbb{R} such that the restriction to any cube of \mathcal{C}_p is a polynomial of degree up to n . Since $\mathcal{P}_L \subset \tilde{\mathcal{P}}_n^l$, there holds

$$\inf_{p \in \tilde{\mathcal{P}}_n^l} \|f - p\|_{\infty, A} \leq \inf_{p \in \mathcal{P}_L} \|f - p\|_{\infty, A}. \quad (\text{B.3})$$

Since f is definable, [Proposition 1](#) yields a finite collection \mathcal{W} of cells $\mathcal{M} \subset \mathbb{R}^d$, such that each cell is open, definable, full-dimensional, any two cells are disjoint, and the union of the closure of the cells is A . Then, define the following subsets of \mathcal{C}_p :

$$\mathcal{C}_p^U = \{c \in \mathcal{C}_p : \exists \mathcal{M} \in \mathcal{W}, c \subset \mathcal{M}\}, \quad \mathcal{C}_p^V = \mathcal{C}_p \setminus \mathcal{C}_p^U. \quad (\text{B.4})$$

We have the following:

$$\inf_{p \in \mathcal{P}_L} \|f - p\|_{\infty, A} = \inf_{p \in \mathcal{P}_L} \max \left(\max_{c \in \mathcal{C}_p^U} \|f - p\|_{\infty, c}, \max_{c \in \mathcal{C}_p^V} \|f - p\|_{\infty, c} \right) \quad (\text{B.5})$$

$$= \max \left(\max_{c \in \mathcal{C}_p^U} \inf_{p \in \mathcal{P}_n(c)} \|f - p\|_{\infty, c}, \max_{c \in \mathcal{C}_p^V} \inf_{p \in \mathcal{P}_n(c)} \|f - p\|_{\infty, c} \right). \quad (\text{B.6})$$

The first equality follows from the definition of the infinity norm and that the union of the cubes in \mathcal{C}_p^U and \mathcal{C}_p^V is A . The second equality follow from the independence of the expression of any $p \in \mathcal{P}_L$ on any two distinct cubes of \mathcal{C}_p .

Let c denote a cube in \mathcal{C}_p^U . Since c is contained in a cell \mathcal{M} on which f is C^r , the restriction of f to c is C^r . Therefore, [Proposition B.1](#) applies and yield

$$\inf_{p \in \mathcal{P}_n(c)} \|f - p\|_{\infty, c} \leq \left(\frac{\text{diam}(A)}{L} \right)^d \frac{C_{d,r}}{n^{r-1}} \sum_{j=1}^d \left\| \frac{\partial^r f}{\partial x_j^r} \right\|_{\infty, c} \quad (\text{B.7})$$

for some constant $C_{d,r}$ depending only on d and r .

Let c denote a cube in \mathcal{C}_p^V , and x_0 denote an arbitray point in c . Since f is K -Lipschitz, for any $x \in c$,

$$|f(x) - f(x_0)| \leq K \|x - x_0\|. \quad (\text{B.8})$$

Thus,

$$\|f(x) - f(x_0)\|_{\infty, c} \leq K \sup_{x \in c} \|x - x_0\| \leq K \text{diam}(c) = K \text{diam}(A) L^{-1}. \quad (\text{B.9})$$

Combining the two bounds (B.7) and (B.9), and using $L = \lfloor l/d \rfloor + 1 \geq l/d$ yields

$$\inf_{p \in \mathcal{P}_n^L(A)} \|f - p\|_{\infty, A} \leq \max \left(\frac{\text{diam}(A)^d C_{d,r}}{L^d} \sum_{j=1}^d \left\| \frac{\partial^r f}{\partial x_j^r} \right\|_{\infty, \text{diff}_r(f)}, \frac{K \text{diam}(A)}{L} \right) \quad (\text{B.10})$$

$$= \max \left(\frac{d^d \text{diam}(A)^d C_{d,r}}{l^d} \sum_{j=1}^d \left\| \frac{\partial^r f}{\partial x_j^r} \right\|_{\infty, \text{diff}_r(f)}, \frac{dK \text{diam}(A)}{l} \right) \quad (\text{B.11})$$

$$= \max \left(\frac{C'_1}{l^d n^{r-1}}, \frac{C'_2}{l} \right). \quad (\text{B.12})$$

where $C'_1 = d^d \text{diam}(A)^d C_{d,r} \sum_{j=1}^d \left\| \frac{\partial^r f}{\partial x_j^r} \right\|_{\infty, \text{diff}_r(f)}$ and $C'_2 = dK \text{diam}(A)$. \blacksquare

We can now deduce the result of [Theorem 1](#).

Proof of Theorem 1. Consider a number of pieces k and the highest number of cuts that allow splitting a cube in \mathbb{R}^d in k , that is the highest l such that $k \geq (\lfloor l/d \rfloor + 1)^d$. The bound of [Theorem B.1](#) applies to this situation and yields

$$\inf_{p \in \mathcal{P}_n^{L^d}(A)} \|f - p\|_{\infty, A} \leq \max \left(\frac{\text{diam}(A)^d C_{d,r}}{k} \sum_{j=1}^d \left\| \frac{\partial^r f}{\partial x_j^r} \right\|_{\infty, \text{diff}_r(f)}, \frac{K \text{diam}(A)}{k^{1/d}} \right), \quad (\text{B.13})$$

since $k^{1/d} \geq l/d$, which is the claimed bound. \blacksquare

APPENDIX C. AXIS-ALIGNED REGRESSION FORMULATION

In this section, we introduce a variant of the affine hyperplane regression tree, presented in [Section 4](#), that accommodates using hyperplanes aligned with cartesian for partitioning the space. [Tables 1](#) and [2](#) summarize the hyperparameters and variables of the mixed-integer formulation.

Axis-aligned partition of the space. At each branching node $m \in \mathcal{T}_B$, a hyperplane splits the space in two subspaces

$$a_m^\top x_i - b_m < 0 \quad a_m^\top x_i - b_m \geq 0, \quad (\text{C.1})$$

that will be associated to the left and right children of node m . The parameters $a_m \in \{0, 1\}^d$ and $b_m \in [0, 1]$ are variables of the mixed integer program. In the axis-aligned formulation, the hyperplane is aligned with an axis of the cartesian space. This is enforced by requiring for all branching node $m \in \mathcal{T}_B$ that a_m take boolean values, only one of which is one:

$$\sum_{j=1}^d a_{jm} = 1, \quad 0 \leq b_m \leq 1. \quad (\text{C.2})$$

Since $x_i \in [0, 1]$, there holds $a_m^\top x_i \in [0, 1]$, so that b_m is constrained to $[0, 1]$ without loss of generality.

In order to model the strict inequality in (C.1), we follow Bertsimas & Dunn [4] and introduce the vector $\varepsilon \in \mathbb{R}^d$ of smallest increments between two distinct consecutive values in points $(x_i)_{i=[n_{\text{samp}}]}$ in any dimension:

$$\varepsilon_j = \min \left\{ x_j^{(i+1)} - x_j^{(i)}, \text{ for } i \in [d-1] : x_j^{(i+1)} \neq x_j^{(i)} \right\} \quad (\text{C.3})$$

where $x_j^{(i)}$ is the i -th largest value in the j -th dimension. ε_{\max} is the highest value of ε_j and serves as a tight big-M bound, leading to the formulation

$$a_m^\top x_i \geq b_m - (1 - z_{it}) \quad \forall m \in A_R(t) \quad (\text{C.4})$$

$$a_m^\top (x_i + \varepsilon) \leq b_m + (1 + \varepsilon_{\max})(1 - z_{it}) \quad \forall m \in A_L(t) \quad (\text{C.5})$$

both for all i in $[n_{\text{samp}}]$ and all t in \mathcal{T}_L . Recall that z_{it} takes binary values and is equal to one if sample x_i belongs to leaf node t .

Combining these elements yields the axis-aligned formulation:

$$\min \frac{1}{n_{\text{samp}}} \sum_{i=1}^{n_{\text{samp}}} \delta_i \quad (\text{C.6a})$$

$$\text{s.t. } \delta_i \geq \phi_{it} - (1 - z_{it})M \quad \forall i \in [n_{\text{samp}}], \quad \forall t \in \mathcal{T}_L \quad (\text{C.6b})$$

$$\delta_i \geq -\phi_{it} - (1 - z_{it})M \quad \forall i \in [n_{\text{samp}}], \quad \forall t \in \mathcal{T}_L \quad (\text{C.6c})$$

$$\phi_{it} = y_i - \text{poly}(x_i; c_t) \quad \forall i \in [n_{\text{samp}}], \quad \forall t \in \mathcal{T}_L \quad (\text{C.6d})$$

$$a_m^\top x_i \geq b_m - (1 - z_{it}) \quad \forall i \in [n_{\text{samp}}], \quad \forall t \in \mathcal{T}_L, \quad \forall m \in A_R(t) \quad (\text{C.6e})$$

$$a_m^\top (x_i + \varepsilon) \leq b_m + (1 + \varepsilon_{\max})(1 - z_{it}) \quad \forall i \in [n_{\text{samp}}], \quad \forall t \in \mathcal{T}_L, \quad \forall m \in A_L(t) \quad (\text{C.6f})$$

$$\sum_{t \in \mathcal{T}_L} z_{it} = 1 \quad \forall i \in [n_{\text{samp}}] \quad (\text{C.6g})$$

$$z_{it} \leq l_t \quad \forall i \in [n_{\text{samp}}], \quad \forall t \in \mathcal{T}_L \quad (\text{C.6h})$$

$$\sum_{i=1}^{n_{\text{samp}}} z_{it} \geq N_{\min} l_t \quad \forall t \in \mathcal{T}_L \quad (\text{C.6i})$$

$$\sum_{j=1}^d a_{jt} = 1 \quad \forall t \in \mathcal{T}_B \quad (\text{C.6j})$$

$$0 \leq b_t \leq 1 \quad \forall t \in \mathcal{T}_B \quad (\text{C.6k})$$

$$z_{it}, l_t \in \{0, 1\} \quad \forall i \in [n_{\text{samp}}], \quad \forall t \in \mathcal{T}_L \quad (\text{C.6l})$$

$$a_{jt} \in \{0, 1\} \quad \forall j \in [d], \quad \forall t \in \mathcal{T}_B \quad (\text{C.6m})$$

$$\phi_{it} \in \mathbb{R} \quad \forall i \in [n_{\text{samp}}], \quad \forall t \in \mathcal{T}_L \quad (\text{C.6n})$$

The constraints Eqs. (C.6e)–(C.6m) are the optimal classification trees (OCT) of Bertsimas & Dunn [4], whereas the other constraints are our extensions thereof. Note that we do not use the complexity parameters of the OCT formulation (d_t) and replace them with 1, where appropriate.

APPENDIX D. COMPLEMENTARY EXPERIMENTAL RESULTS

In this section, we give complementary experiments that illustrate the practical behavior of the axis-aligned and affine-hyperplane regression models.

Setup. The setup is identical to the one described in Section 5. We consider three additional regression problems, for which we plot the landscapes in the forthcoming figures and give approximation errors in Table 7.

Table 6: Summary of the variables of the axis-aligned regression tree formulation

variable	index domain	interpretation
$l_t \in \{0, 1\}$	$t \in \mathcal{T}_L$	1 iff any point is assigned to leaf t
$z_{it} \in \{0, 1\}$	$t \in \mathcal{T}_L, i \in [n_{\text{samp}}]$	1 iff point x_i is assigned to leaf t
$a_m \in \{0, 1\}^d$	$m \in \mathcal{T}_B$	coefficients of the axis-aligned cut
$b_m \in \mathbb{R}$		
$\phi_{it} \in \mathbb{R}$	$t \in \mathcal{T}_L, i \in [n_{\text{samp}}]$	fit error of point x_i by the polynomial of leaf t
$\delta_i \in \mathbb{R}$	$i \in [n_{\text{samp}}]$	fit error of point x_i by the piecewise polynomial function
$c_t \in \mathbb{R}^{\binom{n+d-1}{d-1}}$	$t \in \mathcal{T}_L$	coefficients of the degree n polynomial associated with leaf t

Piecewise-linear norms. We consider two simple piecewise linear test functions: the $\|\cdot\|_1$ and $\|\cdot\|_\infty$ norms, defined for $x \in \mathbb{R}^d$ by

$$\|x\|_1 = \sum_{i=1}^d |x_i|, \quad \|x\|_\infty = \max_{i \in [d]} |x_i|. \quad (\text{D.1})$$

For both functions, we set depth $D = 2$ and polynomial degree $n = 1$. We sample $n_{\text{samp}} = 250$ points in the approximation space. We test both the axis-aligned (C.6) and the general affine-hyperplane (19) formulations with a time limit of 5 minutes for each optimization. For both norms, the axis-aligned formulation was solved to optimality and the affine-hyperplane formulation timed out.

Figure 9a shows the results on the $\|\cdot\|_1$ norm. Note that the full-dimensional cells of the $\|\cdot\|_1$ are axis aligned, so the axis-aligned formulation (C.6) (with $D = 2$) recovers both the correct cells and the correct polynomial function on each piece. The more general affine-hyperplane formulation (19) with performs equally well.

Figure 9b shows the results for the $\|\cdot\|_\infty$. The axis-aligned formulation (C.6) with depth yields a piecewise polynomial function that performs poorly at approximating the function. This is reasonable, as the full-dimensional cells are not axis-aligned anymore. The affine-hyperplane formulation (19) yields a piecewise polynomial function that matches the cells of the function, as well as the polynomial expression of the function on the cells.

Numerical results for both norms are in Table 7. They show a slight increase in error when using the affine-hyperplane formulation on the $\|\cdot\|_1$ norm. This can be attributed to the fact that the true partitioning is axis-aligned, which agrees with the main limitation of the axis-aligned formulation. And because the axis-aligned formulation is simpler to optimize, we obtain a provably optimal solution. Despite that, the solution of affine-hyperplane formulation has only slightly worse error. Additionally, looking at the errors for the $\|\cdot\|_\infty$ norm, we see order(s) of magnitude improvements in the error, when using the affine-hyperplane formulation. This underlines the increased expressivness of the more general formulation. An additional Neural Network approximation. Much as described in Section 5, we consider a similar NN with 25 parameters (2 hidden layers with 4 and 2 neurons respectively), but with *only* ReLU activation functions. The network is trained to minimize the mean squared error with the 2-dimensional function $x \mapsto 2 \sin x_1 + 2 \cos x_2 + x_2/2$ taken at 10 random points from the input space. All data is processed in a single batch, for 5000 epochs, using AdamW optimizer.

The piecewise linear approximation is obtained from the affine-hyperplane formulation with depth $D = 2$ and $n_{\text{samp}} = 225 = 15^2$ sample points (shown as red crosses) placed on a regular grid of 15×15 points. The degree of the polynomial pieces is $n = 1$. The MIP optimization times out after 5 minutes.

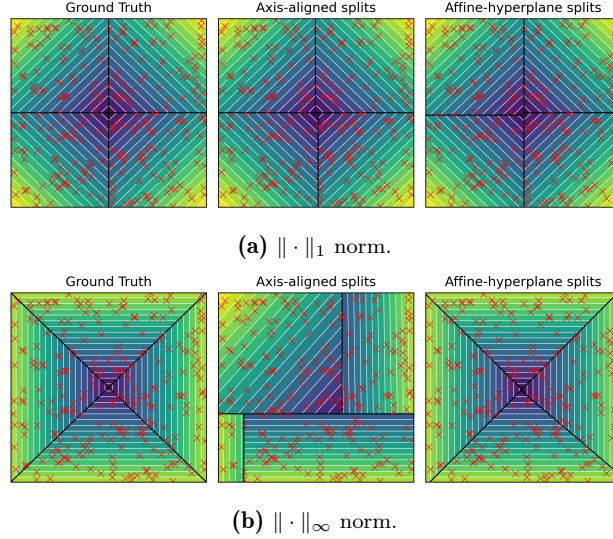


Figure 9: Results on norm functions. On the left are the original functions, middle column contains the results of the axis-aligned formulation (C.6) and on the right are results of the more general affine-hyperplane formulation (19) from the main body of the paper. Red crosses are the coordinates of samples used in the optimization. White lines are the level lines of the function values. Black lines show the partitioning of the space.

Table 7: Normalized absolute error between the functions and their approximations by the axis-aligned (C.6) and affine-hyperplane trees (19) of depth 2. The error is computed on a 1000×1000 grid of regularly spaced points. We divide the absolute errors by the maximal absolute value of the underlying ground truth to improve comparability.

Test function	Axis-aligned tree (C.6)			Affine-hyperplane tree (19)		
	max. err.	mean err.	median err.	max. err.	mean err.	median err.
$\ \cdot\ _1$	2.2×10^{-2}	9.8×10^{-5}	3.0×10^{-5}	2.6×10^{-2}	1.1×10^{-4}	3.0×10^{-5}
$\ \cdot\ _\infty$	7.2×10^{-1}	8.5×10^{-2}	2.8×10^{-2}	6.6×10^{-2}	4.2×10^{-4}	5.0×10^{-5}
ReLU NN	-	-	-	3.0×10^{-2}	1.8×10^{-4}	2.7×10^{-7}

Figure 10a shows the landscape of the network in the left pane and the piecewise linear approximation in the right pane. The obtained piecewise polynomial function essentially recovers the cell decomposition of the network. Figure 10b presents the difference between the NN output and the approximation. The approximation recovers the slope of the network correctly on each of the cells. The discrepancy between the two functions is caused by the slight mismatch between the cell decomposition of the network and its approximation, which could arguably be improved by taking samples from a denser grid.

Looking at the last row of Table 7, we notice that the median error is the lowest among all functions by orders of magnitude, pointing to the high quality of the fit of the polynomials in each partition. This might be due to the properties of taking points on a regular grid which might allow for better approximation.

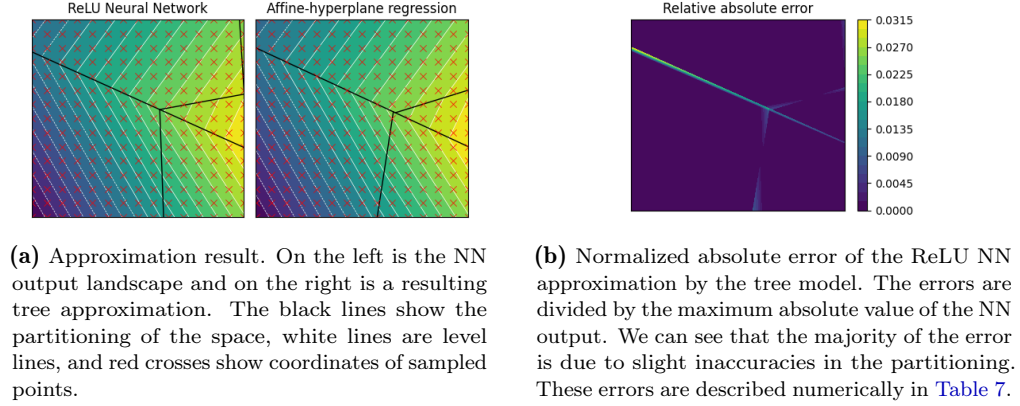


Figure 10: Approximation of the Neural Network with only ReLU activations. On the left, in Figure 10a, is the original output and the approximation. Figure 10b, on the right, shows the normalized absolute error between the two functions.

ACKNOWLEDGMENTS

This work has received funding from the European Union’s Horizon Europe research and innovation programme under grant agreement No. 101070568. This work received funding from the National Centre for Energy II (TN02000025).

REFERENCES

- [1] Aravanis, C., Aspmann, J., Korpas, G., and Marecek, J. Polynomial matrix inequalities within tame geometry. *arXiv preprint arXiv:2206.03941*, 2022.
- [2] Aspmann, J., Korpas, G., and Marecek, J. Taming binarized neural networks and mixed-integer programs. *arXiv preprint arXiv:2310.04469*, 2023.
- [3] Bernstein, S. Sur la meilleure approximation de $|x|$ par des polynomes de degrés donnés. *Acta Mathematica*, 37(1):1–57, December 1914. ISSN 1871-2509. doi: 10.1007/BF02401828.
- [4] Bertsimas, D. and Dunn, J. Optimal classification trees. *Machine Learning*, 106(7):1039–1082, July 2017. ISSN 1573-0565. doi: 10.1007/s10994-017-5633-9.
- [5] Bianchi, P., Hachem, W., and Schechtman, S. Stochastic subgradient descent escapes active strict saddles on weakly convex functions. *Mathematics of Operations Research*, 2023.
- [6] Boissonnat, J.-D., Kachanovich, S., and Wintraecken, M. Tracing Isomanifolds in \mathbb{R}^d in Time Polynomial in d Using Coxeter-Freudenthal-Kuhn Triangulations. pp. 16 pages, 1972902 bytes, 2021. ISSN 1868-8969. doi: 10.4230/LIPICS.SOCG.2021.17.
- [7] Bolte, J. and Pauwels, E. A mathematical model for automatic differentiation in machine learning. In *Advances in Neural Information Processing Systems*, volume 33, pp. 10809–10819. Curran Associates, Inc., 2020.
- [8] Bolte, J. and Pauwels, E. Conservative set valued fields, automatic differentiation, stochastic gradient methods and deep learning. *Mathematical Programming*, 188:19–51, 2021.
- [9] Bondar, D. I., Popovych, Z., Jacobs, K., Korpas, G., and Marecek, J. Recovering models of open quantum systems from data via polynomial optimization: Towards globally convergent quantum system identification. *arXiv preprint arXiv:2203.17164*, 2022.
- [10] Chatterjee, S. and Goswami, S. Adaptive estimation of multivariate piecewise polynomials and bounded variation functions by optimal decision trees. *The Annals of Statistics*, 49(5): 2531–2551, October 2021. ISSN 0090-5364, 2168-8966. doi: 10.1214/20-AOS2045.

- [11] Coste, M. *An Introduction to O-minimal Geometry*. Istituti Ed. e Poligrafici Intern, Pisa, 2000. ISBN 978-88-8147-226-0.
- [12] Dai, F. and Prymak, A. Polynomial approximation on \mathbb{C}^2 -domains. *Constructive Approximation*, pp. 1–52, 2023.
- [13] Davis, D., Drusvyatskiy, D., Kakade, S., and Lee, J. D. Stochastic Subgradient Method Converges on Tame Functions. *Foundations of Computational Mathematics*, 20(1):119–154, February 2020. ISSN 1615-3383. doi: 10.1007/s10208-018-09409-5.
- [14] Davis, D., Drusvyatskiy, D., and Jiang, L. Active manifolds, stratifications, and convergence to local minima in nonsmooth optimization. *arXiv preprint arXiv:2108.11832*, 2021.
- [15] Ditzian, Z. and Totik, V. *Moduli of smoothness*, volume 9. Springer Science & Business Media, 2012.
- [16] Donoho, D. L. Cart and best-ortho-basis: a connection. *The Annals of Statistics*, 25(5): 1870–1911, 1997.
- [17] Goldberg, N., Rebennack, S., Kim, Y., Krasko, V., and Leyffer, S. MINLP formulations for continuous piecewise linear function fitting. *Computational Optimization and Applications*, 79(1):223–233, May 2021. ISSN 1573-2894. doi: 10.1007/s10589-021-00268-5.
- [18] Hanin, B. and Rolnick, D. Complexity of linear regions in deep networks. In Chaudhuri, K. and Salakhutdinov, R. (eds.), *Proceedings of the 36th International Conference on Machine Learning*, volume 97 of *Proceedings of Machine Learning Research*, pp. 2596–2604. PMLR, 09–15 Jun 2019. URL <https://proceedings.mlr.press/v97/hanin19a.html>.
- [19] Helmer, M. and Nanda, V. Conormal Spaces and Whitney Stratifications. *Foundations of Computational Mathematics*, 23(5):1745–1780, October 2023. ISSN 1615-3383. doi: 10.1007/s10208-022-09574-8.
- [20] Helmer, M. and Nanda, V. Effective Whitney Stratification of Real Algebraic Varieties, July 2023.
- [21] Huchette, J. and Vielma, J. P. Nonconvex Piecewise Linear Functions: Advanced Formulations and Simple Modeling Tools. *Operations Research*, 71(5):1835–1856, September 2023. ISSN 0030-364X. doi: 10.1287/opre.2019.1973.
- [22] Iutzeler, F. and Malick, J. Nonsmoothness in Machine Learning: Specific Structure, Proximal Identification, and Applications. *Set-Valued and Variational Analysis*, 28(4):661–678, December 2020. ISSN 1877-0533, 1877-0541. doi: 10.1007/s11228-020-00561-1.
- [23] Jekel, C. F. and Venter, G. *pwlfit: A Python Library for Fitting 1D Continuous Piecewise Linear Functions*, 2019. URL https://github.com/cjekel/piecewise_linear_fit_py.
- [24] Jozs, C. Global convergence of the gradient method for functions definable in o-minimal structures. *Mathematical Programming*, February 2023. ISSN 1436-4646. doi: 10.1007/s10107-023-01937-5.
- [25] Kazda, K. and Li, X. Nonconvex multivariate piecewise-linear fitting using the difference-of-convex representation. *Computers & Chemical Engineering*, 150:107310, 2021. ISSN 0098-1354. doi: <https://doi.org/10.1016/j.compchemeng.2021.107310>. URL <https://www.sciencedirect.com/science/article/pii/S0098135421000880>.
- [26] Kurdyka, K. On gradients of functions definable in o-minimal structures. *Annales de l’Institut Fourier*, 48(3):769–783, 1998. ISSN 1777-5310. doi: 10.5802/aif.1638.
- [27] Lê Loi, T. Verdier and strict thom stratifications in o-minimal structures. *Illinois Journal of Mathematics*, 42(2):347–356, 1998.
- [28] Liu, Y., Cole, C. M., Peterson, C., and Kirby, M. Relu neural networks, polyhedral decompositions, and persistent homology. In *Topological, Algebraic and Geometric Learning Workshops 2023*, pp. 455–468. PMLR, 2023.
- [29] Madrid Padilla, O. H., Yu, Y., and Rinaldo, A. Lattice partition recovery with dyadic cart. In Ranzato, M., Beygelzimer, A., Dauphin, Y., Liang, P., and Vaughan, J. W. (eds.), *Advances in Neural Information Processing Systems*, volume 34, pp. 26143–26155. Curran

- Associates, Inc., 2021. URL https://proceedings.neurips.cc/paper_files/paper/2021/file/dba4c1a117472f6aca95211285d0587e-Paper.pdf.
- [30] Pleśniak, W. Extension and polynomial approximation of ultradifferentiable functions in RN. *Bulletin de la Société Royale des Sciences de Liège*, 63(5):393–402, 1994. ISSN 0037-9565.
 - [31] Pleśniak, W. Multivariate Jackson Inequality. *Journal of Computational and Applied Mathematics*, 233(3):815–820, December 2009. ISSN 0377-0427. doi: 10.1016/j.cam.2009.02.095.
 - [32] Rannou, E. The Complexity of Stratification Computation. *Discrete & Computational Geometry*, 19(1):47–78, January 1998. ISSN 0179-5376. doi: 10.1007/PL00009335.
 - [33] Serra, T., Tjandraatmadja, C., and Ramalingam, S. Bounding and Counting Linear Regions of Deep Neural Networks. In *Proceedings of the 35th International Conference on Machine Learning*, pp. 4558–4566. PMLR, July 2018.
 - [34] Totik, V. Polynomial approximation in several variables. *Journal of Approximation Theory*, 252:105364, 2020.
 - [35] Van den Dries, L. *Tame topology and o-minimal structures*, volume 248. Cambridge university press, 1998.
 - [36] Vielma, J., Ahmed, S., and Nemhauser, G. Mixed-Integer Models for Nonseparable Piecewise-Linear Optimization: Unifying Framework and Extensions. *Operations Research*, 58:303–315, April 2010. doi: 10.1287/opre.1090.0721.
 - [37] Warwicker, J. and Rebennack, S. A Comparison of Two Mixed-Integer Linear Programs for Piecewise Linear Function Fitting. *INFORMS Journal on Computing*, 34, December 2021. doi: 10.1287/ijoc.2021.1114.
 - [38] Warwicker, J. A. and Rebennack, S. Generating optimal robust continuous piecewise linear regression with outliers through combinatorial Benders decomposition. *IIE Transactions*, 55(8):755–767, August 2023. ISSN 2472-5854, 2472-5862. doi: 10.1080/24725854.2022.2107249.